Proceedings of 2018 IEEE/RSJ International Conference on Intelligent Robots and Systems (IROS)
Madrid, Spain, October 1-5, 2018

User-Adaptive Human-Robot Formation Control for an Intelligent Robotic Walker using Augmented Human State Estimation and Pathological Gait Characterization

Georgia Chalvatzaki, Xanthi S. Papageorgiou, Petros Maragos and Costas S. Tzafestas
School of Electrical and Computer Engineering, National Technical University of Athens, Greece
{gchal,xpapag}@mail.ntua.gr, {maragos,ktzaf}@cs.ntua.gr

Abstract— **In this paper we describe a control strategy for a user-adaptive human-robot system for an intelligent robotic Mobility Assistive Device (MAD) using raw data from a single laser rangefinder (LRF) mounted on the MAD and scanning the walking area. The proposed control architecture consists of three modules. In the first module, a previously proposed methodology (termed IMM-PDA-PF) delivers the augmented human state estimation of the user by providing robust leg tracking and on-line estimation of the human gait phases. This information is processed at the next module for providing the pathological gait parametrization and characterization, by computing specific gait parameters for each gait cycle. These gait parameters form the feature vector that classifies the user in a certain class related to risk of fall. Those are of particular significance to the system, since the gait parameters and the respective class are used in the third module, i.e. the human-robot formation controller, in order to adapt the desired formation of the human-robot system, by selecting the appropriate control variables. The experimental evaluation comprises gait data from real patients, and demonstrates the stability of the human-robot formation control, indicating the importance of incorporating an on-line gait characterization of the user, using non-wearable and non-invasive methods, in the context of a robotic MAD.**

I. INTRODUCTION

In a robotic society, elderly people shall not be excluded by the benefits of technological innovation, that could ameliorate their living standards. It is common knowledge that as life expectancy increases, the elderly population keeps rising. One important issue that elders face are mobility problems. Ageing induces instability and lower walking speed and generally affects basic gait parameters of normal subjects, while also changes in stride length and gait patterns are caused by certain pathologies [1]. The gait speed is associated with the functional independence and mobility impairment of the elderly [2], and is therefore closely connected to fall incidents. Robotics fit naturally to the role of assistance, since it can incorporate features such as posture support and stability, walking assistance, health monitoring, etc.

These goals closely interweave; while the ethical goal is to increase the user mobility, its constraint leads to user dissatisfaction, anxiety and frustration, and finally rejection of the system. Therefore, a common research topic in recent years is the development of robotic Mobility Assistive Devices (MADs) for elders that provide physical, sensorial and cognitive assistance [3]. Our aim is to use intelligent MADs (Fig.1), which can monitor and understand the patient's walking state and will autonomously reason on performing assistive actions regarding the patient's mobility. For a robotic MAD that aims to support patients of different mobility status and also assist their rehabilitation progress, user-adaptation is important, meaning that a deployable MAD system should be able to assess the mobility state of the user and adapt its strategies accordingly. A smart MAD should also serve the purposes of medical monitoring, contributing to rehabilitation progress and fall prevention.

This research work has been partially supported by two EU-funded Projects: BabyRobot (H2020, grant agreement no. 687831) and I-SUPPORT (H2020-PHC-19-2014, grant agreement no. 643666).

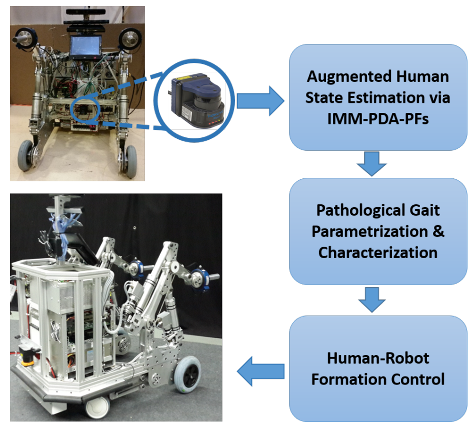

Fig. 1: The control architecture of a user-adaptive control framework that was developed for the depicted robotic MAD, constructed with financial support of EU project MOBOT, equipped with a LRF aiming to record the gait data of the user (below knee level).

In literature, there exist MAD control strategies such as adaptive admittance control schemes [4]. In [5] an admittance control is presented for a passive walker considering the position and velocity of the user, utilizing measurements from a Laser Range Finder (LRF). A control strategy that used as inputs the linear/angular velocities and the orientation of the human and the walker, using data from force/torque sensors, a LRF mounted on the walker and a wearable IMU on the user is presented in [6]. A formation control was presented in [7] for safely navigating blind people, using as input the torso point-cloud. An adaptive shared control for a robotic MAD is presented in [8], using as input user-data from force/torque sensors on the handles and the LRF that detects obstacles. In our previous work [9], we have provided significant findings regarding the impact of different generic control designs on the patient's gait status, by experimentally validating the affect of custom-made control designs on the patient's walking performance, relative to his medical categorization (POMA score [10]). By estimating certain gait parameters, we have shown that subjects with low and moderate mobility function were affected negatively, while subjects with higher mobility function did not seem to present significant change in their gait. Therefore, we have justified the necessity of incorporating a gait assessment system on the MAD's control strategy.

For extracting gait motions, different types of sensors have been used [11], [12]. The development of a low-cost pathological walking assessment tool was presented in [13]. Gait analysis can be achieved by using Hidden Markov Models for modelling normal [14] and pathological human gait [15], and extracting gait parameters [16]. Gait parameters are commonly used for medical diagnosis and are also associated with fall risk prediction. Recently, we have developed a new method for online augmented human state estimation, that uses Interacting Multiple Model Particle Filters with Probabilistic Data Association (IMM-PDA-PFs) [17], which tracks the users' legs using data from a LRF, while it provides real-time gait phase estimation.

In this work, we propose an implementation of a user-adaptive robot control architecture to meet the special needs of people with variable motor inabilities, using data from a single LRF that is mounted on the MAD of Fig. 1, to track the user. The augmented human state estimation method of [17], provides robust leg tracking and real-time gait phases estimation. A pathological gait parametrization and characterization is provided by an on-line system that extracts gait parameters and employs them to classify the subject to a pathological class, which is associated with risk of fall. In such a framework the real-time gait status assessment triggers assistive actions and behaviours. i.e. velocity adjustment, approach of the patient due to changes in gait patterns, etc. For the user-adaptive human-robot formation controller, we use as input the kinematic state of the user's legs, the respective gait parameters of each gait cycle and the pathological class to define the appropriate variables for the human-robot system.

We present a thorough analysis of the methodological framework for such a control strategy, that uses input from a single LRF, i.e. a non-wearable sensor and thus, constitutes a non-invasive method for a robotic MAD, that can be used both in supporting and following modes of the robotic assistant. We experimentally validate the efficacy of the pathological gait parametrization and characterization in providing accurate pathological gait status classification of the user. Moreover, we justify the stability of the human-robot system, that adapts its variables according to the selected pathological class of the user, by providing results from simulations of the human-robot formation using recorded gait data from real patients.

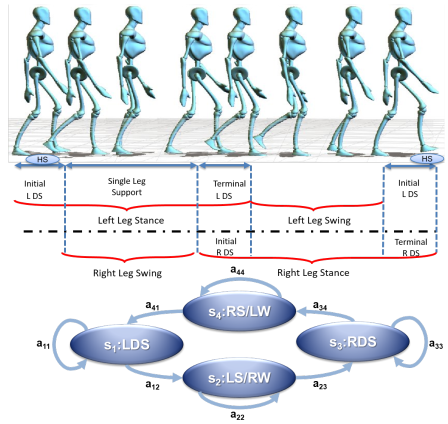

Fig. 2: On top: human gait cycle representation regarding Single Leg or Double Leg Support (DS). Below: The gait IMM as a first-order Markov chain that represents the possible transitions for the human gait states.

II. CONTROL ARCHITECTURE

In Fig. 1 the architecture of the proposed control strategy is presented for the depicted MAD, that aims to provide optimal support and assist with rehabilitation. The data are provided by a LRF mounted on the MAD, which scans the walking area. The raw data are processed at a higher level by an Augmented Human State Estimation module that uses an IMM-PDA-PF framework to track the user's legs and also, provides gait phase estimation in real-time. This information is used in the next module for the Pathological Gait Characterization of the user by employing the information from the gait phases estimation to segment gait cycles and provide on-line computation of the gait parameters. Each time a gait cycle completes, specific gait parameters are computed and form the feature vector of a classifier that categorizes the current gait cycle to a certain pathological gait class. The higher and medium levels feed the last module that comprises a human-robot formation controller. The desired formation is associated with the pathological class, as also the user's augmented state estimates along with the extracted gait parameters are used to define the appropriate control input variables of the human-robot system to achieve user-adaptive control of the MAD.

A. Augmented Human State Estimation using IMM-PDA-PFs

For the augmented human state estimation, we have proposed in [17] a novel framework for efficient and robust leg tracking along with estimating the human gait state, i.e. the respective gait phase at each time instant. This approach uses two Particle Filters (PFs) and Probabilistic Data Association (PDA) with an Interacting Multiple Model (IMM) scheme for a real-time selection of the appropriate motion model according to the human gait analysis and the use of the Viterbi algorithm for an augmented human gait state estimation. The gait state estimates also interact with the IMM as a prior information that drives the Markov sampling process, while the PDA ensures that the legs of the same person are coupled.

The IMM is inspired by human gait analysis [18], incorporating the two main periods in each gait cycle, the stance and swing phases. The stance period can be subdivided into three internal time intervals, Fig. 2: the initial Double Support (DS): begins with Heel Strike (HS) and is the time when both feet are on the ground; the single leg support: when only one leg is at stance while the opposite leg is swinging; the terminal DS: begins with the HS of the opposite foot.

The gait cycle can be seen as an interacting model. Thus, the gait IMM is the first-order Markov model of the human gait states, Fig. 2, i.e. the discrete states s_i, $i = 1,..,4$ and the possible transitions a_{ij} from s_i to s_j for $i, j = 1,..,4$, where LDS: "Left Double Support", LS/RW: "Left Stance/ Right Swing", RDS: "Right Double Support" and RS/LW: "Right Stance/ Left Swing". Each state s_i refers to both legs and imposes a different motion model, i.e. it alters the motion models of the PFs. The legs are tracked, and a maximum likelihood estimation of a human-centered state vector to belong to a gait state is computed. The gait state estimate drives the Markov sampling from the IMM for the next time frame. A thorough analysis of the IMM-PDA-PF methodology is provided in [17].

B. Pathological Gait Parametrization & Characterization

The ultimate goal is to adapt the MAD's controller to the user's needs and pathological condition. Towards this end, we employ the results of the IMM-PDA-PFs methodology regarding the human gait phase estimation, to segment in real-time gait cycles and extract specific gait parameters used for medical diagnosis [19]. Having the recognized gait cycles and their internal phases (each gait state is related to a certain time instant, assisting in the temporal segmentation of the gait cycles), defined in Fig. 2, along with the legs' kinematic states from the IMM-PDA-PF, we can compute gait parameters, like the spatial parameters stride length, step length, gait speed and temporal parameters like stride time, stance/swing time and step time.

Due to our goal to classify the patient's mobility status and also extract those parameters that are important to the human-robot formation control, we choose to compute the following parameters that also serve as the feature vector for an appropriate classifier: 1) *stride length*, 2) *gait speed*, 3) *stance time*, 4) *ratio of stance to stride time*, 5) *ratio of swing to stride time*, 6) *ratio of left step to right step length* and 7) *Double Support time*.

In this work, we aim to categorize the subjects into two classes regarding their risk of fall, in order to use this information as an indicator that will help us decide over the appropriate control parameters of the human-robot system. The subjects' grouping into those classes is associated with their POMA scores, which was provided by clinical evaluation of the medical experts. According to literature [20], subjects with POMA score less than 18 present high risk of falling, while a POMA score between 19 and 23 indicates a moderate risk of fall. Therefore, for this binary classification problem, we use the simple yet effective in such cases SVM classifier [21], for the feature vector of gait parameters that was described previously. Each pathological class triggers the selection of different control variables for the human-robot formation control, thus adapting the system to the specific needs of the user.

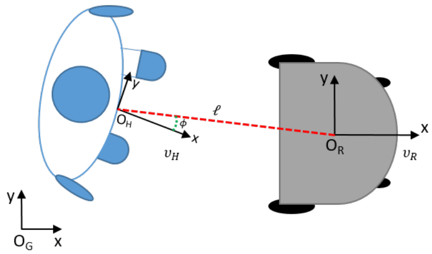

Fig. 3: Human-Robot Formation and parameters.

C. Human-Robot Formation Control

We assume that the human and robot's kinematics can be abstracted as a unicycle. Let $\mathbf{x}_n = [x_n, y_n, \theta_n]^T \in \mathbb{SE}(2)$ be the state vector of human/robot, where $n = \{H, R\}$ denoting human and robot respectively, (x_n, y_n) are the position coordinates and θ_n the orientation. The kinematics are given by: $\dot{x}_n = \upsilon_n \cos\theta_n$, $\dot{y}_n = \upsilon_n \sin\theta_n$, $\dot{\theta}_n = \omega_n$, where υ_n, ω_n are the linear and angular velocity respectively of the n^{th} agent.

Inspired by the leader-follower formation control, we develop a framework consisting of a feedback controller for the human-robot system. The formation control incorporates the control of relative positions and orientations of the human and the robotic assistant, while allowing them to move as a whole. The leader defines the motion and the follower is controlled to follow the leader's motion by keeping a desired separation and a desired relative bearing. In our case, the leader, i.e. the one imposing the motion, is the human and the follower is the robot, forming a front-following formation problem. Let ℓ^d be the desired separation and ϕ^d the desired relative bearing. The relative bearing is defined as the clockwise angle from the heading of the human to the straight line connecting the human to the robot's reference frame. The human-robot system, shown in Fig. 3, is transformed to new coordinates according to a global reference frame O_G, and the human state is the input of the system. The kinematic equation that describes the human-robot formation is:

$$\begin{aligned} \dot{\mathbf{w}} &= A(\mathbf{w}, \beta) \cdot \mathbf{u}_R + B(\mathbf{w}) \cdot \mathbf{u}_H \\ \dot{\beta} &= \omega_H - \omega_R \end{aligned} \tag{1}$$

where $\mathbf{w} = \begin{bmatrix} \ell & \phi \end{bmatrix}^T$ is the system's state, β is the relative orientations, $\mathbf{u}_H = [\ \upsilon_H \quad \omega_H]^T$ is the human velocity vector, and $\mathbf{u}_R = [\ \upsilon_R \quad \omega_R]^T$ is the input to the robot. The matrices A and B are defined as follows:

$$A = \begin{bmatrix} \cos(\psi) & b \cdot \sin(\psi) \\ -\frac{1}{\ell}\sin(\psi) & \frac{b}{\ell}\cos(\psi) \end{bmatrix} \quad B = \begin{bmatrix} -\cos(\phi) & 0 \\ \frac{1}{\ell}\sin(\phi) & -1 \end{bmatrix} \tag{2}$$

where $\psi = \beta + \phi$, and b is a positive bias. The control velocity vector $\mathbf{u}_R$ is estimated by applying input-output feedback linearization in (1), which delivers:

$$\mathbf{u}_R = A^{-1} \cdot (\mathbf{q} - B \cdot \mathbf{u}_H) \tag{3}$$

where $\mathbf{q}$ is an auxiliary vector such that:

$$\mathbf{q} = K \cdot (\mathbf{w}^d - \mathbf{w}) \tag{4}$$

where $K = \begin{bmatrix} k_1 & 0 \\ 0 & k_2 \end{bmatrix}$, with $k_1, k_2 > 0$ are positive gains. Also, matrix A is invertible as long as $b/l > 0$, which is always true. The closed-loop linearised system is:

$$\left\{ \begin{array}{l} \dot{\mathbf{w}} = \mathbf{q} = K \cdot (\mathbf{w}^d - \mathbf{w}) \\ \dot{\beta} = \omega_H - \omega_R \end{array} \right\} \tag{5}$$

Under suitable assumptions the human-robot system is stable, meaning that in (5) the output $\mathbf{w}$ converges exponentially to the desired $\mathbf{w}^d$. The stability analysis of this system is proved in [22].

This human-robot system is closely connected to the gait parametrization and characterization for the identification of the control variables. Each time a gait cycle completes, the extracted gait features are used for the real-time classification of the user. Each class induces a different desired separation distance l^d, that is related to the class stride length average measures. We aim to assure that the human-robot formation adapts to changes in gait when for example a subject feels more confident and speeds up their gait, or another subject alternates their gait due to fatigue.

The human linear velocity υ_H is the estimated gait speed that results at the end of each gait cycle. As human position we regard the midpoint of the estimated left and right leg positions and is renewed according to the LRF's frame rate. For the computation of the human angular velocity ω_H, we compute the angle change of the human position w.r.t. the LRF in the relative human-LRF coordinate system. It is true that the human-robot system renews its inputs with different frame rates. On the one hand, the position, orientation and angular velocities are renewed according to the LRF's frame rate, on the other hand the human velocity and the decision of the desired separation distance is connected to the stride time, which also varies from stride to stride. To accommodate the different timings of feeding information to the system, we also applied an Unscented Kalman Filter (UKF) [23] for a human-centred tracking, i.e. a higher level tracking of the human-centred state above the IMM-PDA-PFs.

UKF Human-centred tracking: The tracking framework comprises the well-known UKF, described in [23]. We apply the standard methodology using as state variables the position of the human along the axes x_H, y_H, the orientation θ_H (from which we can compute the angular velocity via differential equation; in the future we will fuse information from the torso rotation to better estimate turning intentions), and the linear velocity υ_H. The state equations are:

$$\begin{array}{l} x_H^t = x_H^{t-1} + \upsilon_H^{t-1} \cdot \cos(\theta_H^{t-1}) \cdot \Delta t \\ y_H^t = y_H^{t-1} + \upsilon_H^{t-1} \cdot \sin(\theta_H^{t-1}) \cdot \Delta t \\ \theta_H^t = \theta_H^{t-1} + \eta_{\theta_H}^t \\ \upsilon_H^t = \upsilon_H^{t-1} + \eta_{\upsilon_H}^t \end{array} \tag{6}$$

where t is the discrete time and $\eta_{\theta_H}^t, \eta_{\upsilon_H}^t$ are the orientation and linear velocity noises modelled as zero-mean white Gaussians with standard deviations $\sigma_\theta = \pi/6$ and $\sigma_\upsilon = 0.02$ m/sec. While the observations for the x_H, y_H, θ_H variables arrive at each laser frame, the velocity observation is held constant for the duration of one gait cycle, therefore till a new velocity observation comes to correct our velocity estimate, we assume the one derived from the prediction step of the UKF as the current velocity prediction. The observation model is linear and the measurement noises for all state variables are also modelled as white Gaussians with standard deviations 0.1 m in position for both axes, $\pi/30$ in orientation and 0.09 m/sec in velocity measurements.

III. EXPERIMENTAL ANALYSIS & RESULTS

A. Experimental data & Evaluation Strategy

The data used in this work derived from real patients who participated in two large scale experiments, conducted in Agaplesion Bethanien Hospital - Geriatric Center, under ethical approval by the ethics committee of the Medical Department of the University of Heidelberg. All subjects had signed written consent for participating in the experiments. The participants presented moderate to mild mobility impairment, according to clinical evaluation. In this work we present two evaluation studies. The first concerns the Pathological Gait parametrization & Characterization Fig. 1, i.e. the pathological gait status classification, while the second one refers to the evaluation of the proposed user-adaptive human-robot formation control strategy. The data used in both studies, were collected by a Hokuyo rapid laser sensor, mounted on the robotic platform of Fig. 1, for the detection of the patients' legs.

For the first experimental evaluation, the subjects have participated in an experiment, where they walked straight for about 3 m in order for medical experts to assess amongst others their POMA scores. The data were collected by the LRF of Fig. 1. Twenty four patients have been categorized in the two classes that we are interested in. We use the gait data from these twenty four patients, that resulted in a dataset of more than 200 strides, in order to train an SVM classifier and validate the classification performance using the features described in Section II-B.

For the formation control evaluation, we simulate a hypothetical unicycle robot, to evaluate the performance of the proposed control architecture given real pathological gait data. For this study, we present data from fourteen patients with unknown POMA scores (their inclusion criterion was only to be of mild/moderate mobility impairment). Those patients were supported by a passive rollator (data collection experiments) equipped with the same type LRF sensor and they had to walk in a free area while making right and left turning manoeuvres.

We provide the analytical formation error results as the average separation distance error, the average relative bearing error and the Euclidean norm of the formation error: $E(t) = P_H(t) - l^d \cdot [\ \cos(\phi^d) \quad sin(\phi^d)]^T$, where $P_H(t) = [x_H, y_H]^T$ is the position of the human along the axis at time instant t, [7]. The control gains in this work are selected after experimentation and are set to be $k_1 = 40$ and $k_2 = 30$. The desired separation for Class 1 was $\ell^d = 0.55$ m and the bias

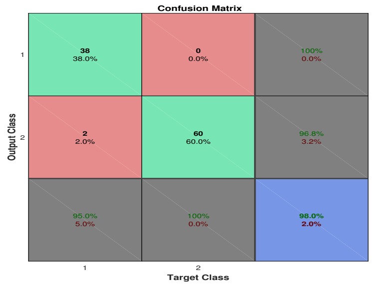

(a) Confusion matrix for the pathological gait classification problem.

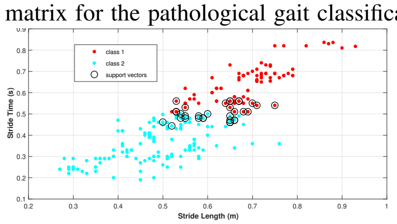

(b) Features stride time vs. stride length for the two classes along with the support vectors at the separation hyperplane.

Fig. 4: Pathological gait classification results.

$b = 0.1$ m, while for Class 2 $\ell^d = 0.75$ m and $b = 0.1$ m. Those parameters have been set using intuition from Table I allowing also a small margin compensating the difference of estimating the step length in the knee level from the actual step length on the foot level, [16]. The initial separation distance regardless of the subject's class was set at 0.6 m. For both studies the IMM-PDA-PF methodology have used a robust implementation of 200 particles [17].

B. Validation of the Pathological Gait Parametrization & Characterization

For justifying the need of the pathological characterization of the users of the intelligent MAD, Table I presents the average measures and standard deviations of the extracted gait features from the whole dataset for each of the two pathological gait classes, which were provided by the medical experts. It is evident that the two classes have very different average measures. For example the average stride lengths differ for about 20 cm, while the average gait speed for Class 1 is almost 25 cm/s less than the respective of Class 2. The stance time is larger in Class 1, while it is interesting that it presents greater variability than in Class 2. Furthermore, the ratios of stance and swing time w.r.t. the stride time are closer to normal for Class 2 (in literature [18] this ratio is 60% stance and 40% swing), while in Class 1 more time is dedicated to stance time, i.e. the subjects of Class 1 are more reluctant in entering the swing phase; following these comments it is natural to also observe a larger DS time in Class 1, a feature that is closely associated with risk of fall. Given these indications regarding the gait features of each class, we proceeded with the training of the SVM classifier, having separated the initial dataset into training and testing sets using a random $70\% - 30\%$ partition.

To train the SVM classifier model we have used the well-known k-fold cross-validation method, for avoiding over fitting problems, over the training dataset using a linear kernel. The cross-validation resulted in a loss, i.e. mean squared error of observations w.r.t. predictions, of about 4%. In Fig. 4a the confusion matrix of the cross-validated SVM over the testing dataset is presented. The classification accuracy in this case was 98%. Furthermore, in Fig. 4b a plot of the features stride time and stride length for both classes is depicted. Marked with red are the features belonging to Class 1, with light blue the ones in Class 2 and the black circles denote the support vectors that define the separation hyperplane of the two classes. It is evident from this plot that the two classes can be linearly separated by an SVM. Although 98% accuracy is high, one can claim that a 2% error is rather high for such an application. However, this error cannot be considered fatal since the classifier runs at the end of each gait cycle, i.e. the class is re-estimated at most every 1.5 sec, while also most of the times these events happen when the features are really close to the separation hyperplane of the classifier. We intend to apply in the future some smoothing on the classifier in order to prevent the abrupt changes of classes and also apply a more sophisticated control approach that will consider certain constraints imposed by the extracted gait parameters.

C. Evaluation of the Human-Robot Formation Control

Table II presents the absolute mean and standard deviation of the formation errors for the separation distance (mm), the relative orientation (deg) and the mean and standard deviation of the norm of the formation error in (mm) of the human-robot system. The results show the convergence of the proposed controller, since the average separation distance error for all patients is approximately 4 mm and the relative bearing error close to 2.5 deg. The mean norm of the formation error $||E||$ is 26 mm and the standard deviation is 17 mm. Furthermore, we present graphical results for two subjects for demonstration purposes.

In Fig. 5 the formation results for subject #1 are presented. In Fig. 5a the trajectories performed in the 2D plane by the subject (red) and the robot (blue) are depicted. The human and robot started at an initial position and performed a trajectory that included right and left manoeuvres along the way and stopped after walking for about 6 m. The green stars indicate the turns along the path performed by the human. In Fig. 5b the evolution of the actual separation distance w.r.t. to the desired one is depicted. It is evident that the controller converges to the desired output, as it is also shown in Table II, where the subject presented average separation distance error of 4 mm. We can also mention after inspecting this figure that the subject was classified at Class 1 for the whole walking activity (the desired distance was constantly set at 0.55 m).

In Fig. 5c the evolution of the relative bearing (deg) w.r.t. the desired value is presented. Cross-examining this figure with the generated human-robot trajectories of Fig. 5a, we can notice that the deviations of the relative bearing from the desired value happen in cases of turning manoeuvres, as for example during time frames from about 30 to 230 that the human makes consecutive right and left turns. However, the

TABLE I: Gait Classification features

Class \ Feature	stride length (m)	gait speed (m/s)	stance time (s)	stance/stride time	swing/stride time	left step/right step length	DS time (s)
Class 1	0.49 ± 0.09	0.39 ± 0.09	0.80 ± 0.23	0.63 ± 0.07	0.37 ± 0.07	0.94 ± 0.24	0.20 ± 0.05
Class 2	0.69 ± 0.07	0.64 ± 0.09	0.61 ± 0.06	0.57 ± 0.03	0.43 ± 0.03	1.01 ± 0.13	0.15 ± 0.04

Average measures and standard deviations of the gait features for Class 1 and Class 2.

TABLE II: Formation Error Results

Error \ Subject	1	2	3	4	5	6	7
distance (mm)	3.9 ± 4.0	4.8 ± 5.5	3.9 ± 7.0	3.8 ± 3.7	5.0 ± 6.9	3.3 ± 3.2	3.6 ± 4.7
bearing (deg)	2.46 ± 1.74	1.84 ± 1.35	1.89 ± 1.75	1.94 ± 1.70	3.03 ± 2.33	2.49 ± 1.55	3.23 ± 2.37
$\|\|E\|\|$ (mm)	31 ± 17	20 ± 11	24 ± 20	21 ± 15	29 ± 21	26 ± 12	25 ± 19
Error \ Subject	**8**	**9**	**10**	**11**	**12**	**13**	**14**
distance (mm)	2.8 ± 6.7	4.4 ± 6.6	3.4 ± 6.3	3.3 ± 3.2	4.3 ± 9.7	3.5 ± 3.3	8.6 ± 8.3
bearing (deg)	1.86 ± 1.25	1.50 ± 1.06	2.14 ± 1.76	2.97 ± 1.96	2.53 ± 1.41	2.39 ± 1.57	4.35 ± 3.16
$\|\|E\|\|$ (mm)	20 ± 12	17 ± 9	22 ± 15	29 ± 18	28 ± 11	22 ± 13	35 ± 24

Average absolute errors and standard deviations for the separation distance, the relative orientation and the norm of formation error E of the human-robot system.

system converges close to the desired bearing for the time frames from about 250 to 400, when the human and robot are walking a straight path, and then again the bearing presents deviations when the human attempts a left turn at the end of the path. Turning manoeuvres can be seen as perturbations to the human-robot system, which the system manages to overcome and converge to the desired value. Even these deviations are admissible for our problem, since they are measured closely to the desired one; subject #1 presented average relative bearing error 2.46 deg, while the affect on the formation error is considered small, since the mean norm of the error $||E||$ for subject #1 is only 31 mm, i.e. a distance that constitutes only the 5% of the desired separation distance for this subject.

In Fig. 6 the formation results for subject #14 are presented. The trajectories executed in the 2D plane by the subject (red) and the robot (blue) are depicted in Fig. 6a. This subject performed a longer path, walking almost 8 m in the horizontal direction, while performing more turns along the way (indicated by the green stars). In Fig. 6b, the evolution of the actual separation distance w.r.t. to the desired one is depicted. The significant remark is that this subject has alternated gait throughout the path. Until the first ~ 150 time frames the subject was classified at Class 1, while for the time frames of about 150 to 320 the subject is classified at Class 2. This time interval corresponds in Fig. 6a at the travel from 2 m to 4 m in the x-direction. It is evident that the user sped up the gait, thus the subject was classified at Class 2, but then again the subject changed the walking performance and was classified at Class 1. Despite the changes between Classes 1 & 2, and the respective alterations in the desired distance separation, the controller converges to the desired output each time, having an average separation distance error of 8.6 mm, which is an admissible error for our application.

In Fig. 6c the evolution of the relative bearing (deg) w.r.t. the desired value is presented. Once more, we cross-examine this figure with the generated human-robot trajectories of Fig. 6a. As this subject performed many turning manoeuvres along the way, there are more deviations of the relative bearing from the desired value. While the system attempts to converge at the desired zero relative bearing, the consecutive perturbations induced by the respective turns, disrupt the system's response. This results in a mean error of 4,35 deg, which is also an admissible error for our case, since the affect on the formation error is considered small, having a mean norm of the error $||E||$ of about 35 mm, i.e. a distance that constitutes approximately 6% over the average desired separation distance (measured at 0.62 m) for the particular subject. In our future work, we will incorporate information regarding the upper body pose and also define certain fall criteria with the help of medical experts.

To our knowledge, the only work in literature that considers a human-robot formation is found in [7], where they used this framework to provide feedback to a tactile sensor worn by blind people. In this implementation, the authors tracked the human torso from a camera point cloud and have set a desired separation distance at 2.3 m. They stated that the mean of the norm of the formation error was 0.52 m, i.e. the error is the 23% of the desired distance, while in our case the errors are much smaller, having a respective percentage error only 4.7%.

IV. CONCLUSIONS AND FUTURE WORK

This paper presents a strategy for user-adaptive human-robot formation control of a robotic MAD, using data from a single LRF mounted on the platform, that scans the walking area. The proposed framework incorporates a robust leg tracking and on-line gait phases estimation using IMM-PDA-PFs, a pathological gait parametrization and characterization module for extracting gait parameters and classifying the user to a class that is associated with risk of fall. Each class defines different control variables for the control of the human-robot system. The proposed controller is inspired by the leader-follower formation control theory. The experimental results presented in this paper show the significance of adapting the human-robot system to the particular pathological gait class of the user and their respective gait parameters, since it is proved to be stable using data from real patients who presented variable gait performance.

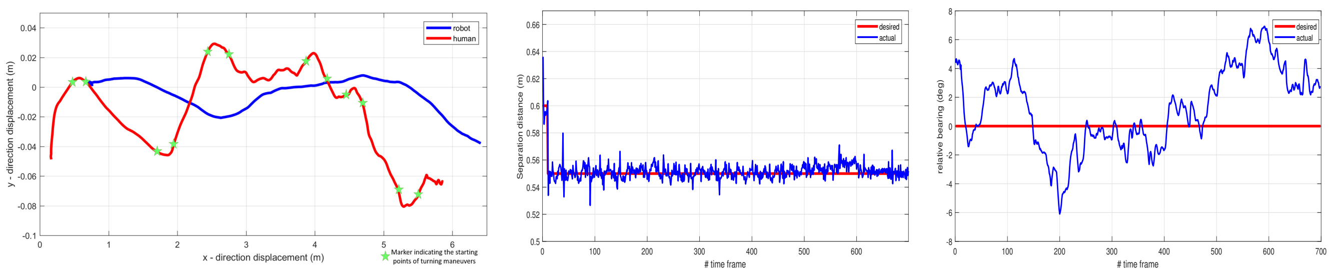

(a) Human-Robot performed trajectories.

(b) Evolution of actual separation w.r.t to desired.

(c) Evolution of actual relative bearing w.r.t to desired.

Fig. 5: Formation results: trajectories, separation distance & relative bearing vs. the desired values for subject #1 (Table II).

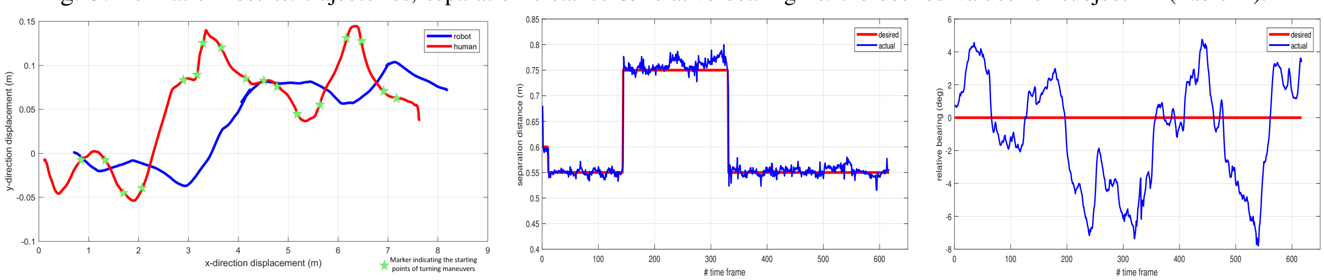

(a) Human-Robot performed trajectories.

(b) Evolution of actual separation w.r.t to desired.

(c) Evolution of actual relative bearing w.r.t to desired.

Fig. 6: Formation results: trajectories, separation distance & relative bearing vs. the desired values for subject #14 (Table II).

In our future work, we aim to apply some constraints on the human-robot system regarding some crucial gait parameters that are closely associated with risk of fall. We are also planning to incorporate an obstacle avoidance control module, and also employ information of the force/torque sensors of the handles in cases of supporting mode of the MAD. Finally, our goal is to test our control strategy with the robotic MAD and patients to evaluate the real-time performance of our framework.

REFERENCES

[1] J. M. Hausdorff, "Gait dynamics, fractals and falls: Finding meaning in the stride-to-stride fluctuations of human walking," *Human Movement Science 2007*.

[2] F. Garcia-Pinillos et. al, "Gait speed in older people: an easy test for detecting cognitive impairment, functional independence, and health state," *Psychogeriatrics*, 2016.

[3] S. Jenkins et. al, "Care, monitoring, and companionship: Views on care robots from older people and their carers," *International Journal of Social Robotics*, 2015.

[4] O. Chuy et. al, "Environment feedback for robotic walking support system control," in *ICRA 2007*.

[5] Y. Hirata et. al, "Motion control of intelligent passive-type walker for fall-prevention function based on estimation of user state," in *ICRA 2006*.

[6] C. A. Cifuentes and A. Frizera, *Development of a Cognitive HRI Strategy for Mobile Robot Control*. Springer International Publishing, 2016.

[7] S. Scheggi et al., "Cooperative human-robot haptic navigation," in *2014 IEEE Int'l Conf. on Robotics and Automation (ICRA)*, May 2014, pp. 2693–2698.

[8] M. Geravand et. al, "An integrated decision making approach for adaptive shared control of mobility assistance robots," *Int'l J. of Social Robotics*, 2016.

[9] G. Chalvatzaki et al., "Towards a user-adaptive context-aware robotic walker with a pathological gait assessment system: First experimental study," in *2017 IEEE/RSJ Int'l Conf. on Intelligent Robots and Systems (IROS)*, Sept 2017, pp. 5037–5042.

[10] M. E. Tinetti, "Performance-oriented assessment of mobility problems in elderly patients," *Journal of the American Geriatrics Society 1986*.

[11] J. Bae and M. Tomizuka, "Gait phase analysis based on a hidden markov model," *Mechatronics*, 2011.

[12] C. Nickel et. al., "Using hidden markov models for accelerometer-based biometric gait recognition," in *CSPA 2011*.

[13] V. Bonnet et. al, "Towards an affordable mobile analysis platform for pathological walking assessment," *Robotics and Autonomous Systems*, 2015.

[14] X. Papageorgiou et. al., "Hidden markov modeling of human normal gait using laser range finder for a mobility assistance robot," in *ICRA 2014*.

[15] ——, "Hidden markov modeling of human pathological gait using laser range finder for an assisted living intelligent robotic walker," in *IROS 2015*.

[16] X. Papageorgiou et. al, "Experimental validation of human pathological gait analysis for an assisted living intelligent robotic walker," in *Biorob 2016*.

[17] G. Chalvatzaki et al., "Augmented human state estimation using interacting multiple model particle filters with probabilistic data association," *IEEE Robotics and Automation Letters*, vol. PP, no. 99, pp. 1–1, 2018.

[18] J. Perry, *"Gait Analysis: Normal and Pathological Function"*, 1992.

[19] A. Muro-de-la-Herran et. al., "Gait analysis methods: An overview of wearable and non-wearable systems, highlighting clinical applications," *Sensors 2014*.

[20] M. Tinetti, "Fall risk index for elderly patients based on number of chronic disabilities," *The American Journal of Medicine*.

[21] N. Cristianini et al., *An Introduction to Support Vector Machines: And Other Kernel-based Learning Methods*. New York, NY, USA: Cambridge University Press, 2000.

[22] A. K. Das et al., "A vision-based formation control framework," *IEEE Trans. on Robotics and Automation*, vol. 18, no. 5, pp. 813–825, Oct 2002.

[23] E. A. Wan et al., "The unscented kalman filter for nonlinear estimation," in *Proc. of IEEE Adaptive Systems for Signal Processing, Communications, and Control Symposium*, 2000, pp. 153–158.